A study of overall contact behavior of an elastic perfectly plastic hemisphere and a rigid plane

He Peng, Zhansheng Liu and Guanghui Zhang

Proceedings of the Institution of Mechanical Engineers, Part J: Journal of Engineering Tribology published online 11 October 2012
DOI: 10.1177/1350650112460799

Original Article

Institution of MECHANICAL ENGINEERS

Journal of ENGINEERING TRIBOLOGY

Proc IMechE Part J: J Engineering Tribology
0(0) 1–16
© IMechE 2012
Reprints and permissions: sagepub.co.uk/journalsPermissions.nav
DOI: 10.1177/1350650112460799
pij.sagepub.com
SAGE

A study of overall contact behavior of an elastic perfectly plastic hemisphere and a rigid plane

He Peng, Zhansheng Liu and Guanghui Zhang

Abstract

The overall contact behavior of an elastic perfectly plastic hemisphere against a rigid plane is presented. Based on volume conservation, the upper limit of overall contact area is derived. A finite element model for the overall contact behavior of a hemisphere and a rigid plane is studied. The material of the hemisphere is assumed to be elastic perfectly plastic. A series of materials with different yield stress to elasticity modulus ratios are studied in finite element analysis. The axial movement of the deformed hemisphere base is prevented. The radial deformable and radial rigid boundary conditions of the hemisphere bottom base are considered. Results show that the overall contact area gradually deviates from Hertz solution, and approaches the upper limit with the increase of interference. Material yield stress to elasticity modulus ratio mainly influences contact behaviors in the early contact stage, while the boundary condition of hemisphere bottom base affects the contact behaviors significantly for large contact interferences. By incorporating some existing models and fitting finite element results, a model for overall contact of a hemisphere against a rigid plane is obtained. This study covers the overall contact, which ranges from initial contact to the collapse of hemisphere. Comparisons of this study with several existing models and experimental data indicate that this study can predict the contact behaviors well in overall contact range.

Keywords

Spherical contact, elastic–plastic, overall, material property, boundary condition

Date received: 18 June 2012; accepted: 17 August 2012

Introduction

The contact behavior of a hemisphere and a rigid flat is one of the fundamental problems in contact mechanics. It can be applied to analyze the contact of asperities on rough surfaces[1–5] in micro-scales and predict the contact of structures with spherical shapes in macro-scales. This study intends to study the overall contact behavior between an elastic perfectly plastic hemisphere and a rigid flat, which ranges from initial contact to the collapse of hemisphere.

Many works on the elastic–plastic contact of a hemisphere against a rigid plane have been published, while the existing models are only valid in part of the overall contact range. The classic Hertz solution[6] predicts the elastic contact behaviors well, and its valid interference range is $0 \leqslant \omega \leqslant \omega_c$, where ω_c is the critical interference which indicates the onset of plastic deformation in hemisphere. The model proposed by Abbott and Firestone[7] (AF) aims at fully plastic contact behaviors of a hemisphere and a rigid plane. However, it cannot predict the mean contact pressure of fully plastic contact well.[8,9] Chaudhri and Yoffe[10] and Chaudhri et al.[11] investigated the elastic and plastic contact of a sphere against rigid flats experimentally. Some models[4,12] bridge Hertz solution and AF model analytically by introducing some assumptions. With finite element analysis, Kogut and Etsion[13] (KE) investigated the evaluation of plastic deformation in the hemisphere in detail and proposed an empirical dimensionless formulation on the elastic–plastic contact behaviors. KE model is valid in the range $0 \leqslant \omega \leqslant 110\omega_c$, which is a small portion of the overall contact. Jackson and Green[8] (JG) proposed an elastic–plastic contact model for a wider range of interferences based on finite element study. Quicksall et al.[14] compared KE and JG models for various material properties and validated that JG model had

School of Energy Science and Engineering, Harbin Institute of Technology, Harbin, People's Republic of China

Corresponding author:
He Peng, School of Energy Science and Engineering, Harbin Institute of Technology, 92 West Dazhi Street, Nan Gang District, Harbin 150001, People's Republic of China.
Email: hepeyfly@foxmail.com

better accuracy for large interferences. Etsion and other researchers[15–17] derived a formulation of the critical interference ω_c analytically and studied the spherical contact behaviors experimentally. Based on experimental study of the fully plastic contact of a sphere against a rigid flat, Jamari and Schipper[9] revealed that the mean contact pressure was constant with load and the contact area was a truncation of the sphere. Shankar and Mayuram[18] proposed an empirical expression on the elastic–plastic contact between a hemisphere and a rigid flat for a larger valid interference range $0 \leqslant \omega \leqslant 450\omega_c$. In order to model the heavily loaded contact behavior of a hemisphere and a rigid plane, Wadwalkar et al.[19] extended JG model with volume conservation assumption. The existing models on the elastic–plastic contact of a hemisphere and a rigid flat are only valid in part of the overall contact range, none of them covers the contact behaviors of the collapsed hemisphere. This study is motivated to study the overall contact behavior of a hemisphere against a rigid flat. The contact surfaces are assumed to be smooth in this study, and the roughness of the hemisphere[20–22] or of the flat[23] will not be considered.

The material properties have influence on the contact behavior of a hemisphere against a rigid flat, especially on elastic–plastic and fully plastic contact. The yield stress Y to elasticity modulus E ratio e_y has significant influence on the elastic–plastic contact behavior. For early elastic–plastic contact, the critical contact behaviors depend on e_y, but the dimensionless models[13,18] are independent of material properties ratio e_y. For heavily elastic–plastic contact and fully plastic contact, the influence of material properties ratio e_y is obvious. Jackson and Green[8] investigated the variation of fully plastic contact pressure with material properties ratio e_y and considered it in the JG model. By comparing the dimensionless models on the contact between a hemisphere and a rigid flat, Quicksall et al.[14] verified that JG model was more accurate for large interferences. Recently, Shankar and Mayuram[18] studied the influence of material properties ratio e_y on the transition behavior of elastic–plastic contact. In the work of Wadwalkar et al.,[19] the influence of material properties ratio e_y on heavily deformed spherical contact was considered as well. From the literature survey, it can be seen that the material yield stress to elasticity modulus ratio e_y has influence on the contact behavior for large interferences. In the study of overall contact behavior of a hemisphere and a rigid plane, the influence of material properties ratio e_y will be considered. The material Poisson's ratio has significant influence on the early evolution of plastic deformation in the hemisphere, while it has little influence on contact area and contact load.[15] Note that the hemisphere material is assumed to be elastic perfectly plastic in this study, the influence of material strain hardening effect[24] will not be considered. Moreover, the elastic perfectly plastic contact behavior studied in this study is different from the hyper elastic contact of a sphere and a rigid, which has been investigated by Raja and Malayalamurthi[25] and Long et al.[26]

According to Saint Venant's principle, the boundary condition of the hemisphere base has little influence on elastic and early stage of elastic–plastic contact.[4,6,8,13] But for heavily deformed contact, the boundary conditions of the hemisphere bottom base have great effect on contact behaviors. In studying the contact behavior of heavily deformed hemisphere, Wadwalkar et al.[19] considered the cases of radial deformable and radial rigid bases. The contact behaviors of the two cases are quite different for large interferences. In the study of elastic–plastic contact of rough surfaces, Zhao and Chang[27] considered the axial deformation of substrate and proposed a model considering the interactions of asperities. Sahoo and Banerjee[28] and Sahoo[29] used this model to study the adhesive contact and friction between rough surfaces. Ciavarella et al.[30] improved Greenwood and Williamson model[1] by considering the deformation of substrate. Yeo et al.[31,32] improved Hertz solution by considering the axial deformation of substrate, and used it to consider the interactions of asperities on rough surface. The radial and axial deformations of hemisphere base both can affect the contact behavior. In this study, the cases of radial deformable and radial rigid boundary conditions of hemisphere base will be studied, while the axial deformation of substrate will not be considered.

Note that this study focuses on the contact between a deformable hemisphere and a rigid flat. It is different from the contact between a rigid sphere and a deformable base, which has been investigated in many works.[33–35] The difference between the two cases was reported by Jackson and Kogut.[36]

This study intends to study the overall contact behavior of an elastic perfectly plastic hemisphere against a rigid plane. The initial elastic contact, elastic–plastic contact, and the collapse of hemisphere are all covered in this study. The upper limit of contact area is derived based on volume conservation. A finite element model for the overall contact behavior of an elastic perfectly plastic hemisphere and a rigid plane is studied. The influences of material yield stress to elasticity modulus ratio and boundary conditions of the hemisphere bottom base are considered. The JG model[8] is adopted for early stage contact, and empirical expressions for other stages are obtained by fitting finite element results. By comparing with some existing models and experimental results, this study can predict the overall contact behavior of an elastic perfectly plastic hemisphere against a rigid plane well.

Theory background

Since this problem is axisymmetric, the hemisphere could be modeled as a quarter of a circle and the rigid flat could be modeled as a rigid line, as shown in Figure 1. The radial movement of the symmetry axis is restrained in this model. The axial deformation of hemisphere base is not considered in this study. Since the radial movement of hemisphere base has significant influences on heavily deformed contact behaviors, the radial deformable and radial rigid bases are considered in this study. As shown in Figure 1(a), the hemisphere base could deformable freely in radial direction. The radial rigid base case is illustrated in Figure 1(b). For radial rigid base case, the deformed hemisphere would pass through the base plane of hemisphere, which is rarely happened practically. Therefore, a rigid plane is added at hemisphere bottom base. Note that the axial deformation of hemisphere base is prevented in this study. For the contact behavior of asperities on rough surfaces, the axial deformation of substrate could be considered using the existing models.[27,30,31]

Two limits of contact area

At initial stage of contact, the hemisphere deforms elastically. Contact area and contact load can be obtained by Hertz solution[6]

$$A_e = \pi R \omega \tag{1}$$

$$F_e = \frac{4}{3} E' R^{\frac{1}{2}} \omega^{\frac{3}{2}} \tag{2}$$

where ω is the contact interference, R the radius of hemisphere, E' the equivalent elasticity modulus of material $E/\left(1-\nu^2\right)$, E the elasticity modulus, and ν the Poisson's ratio.

With the increase of interference, plastic deformation occurs and expands in the hemisphere. Plastic deformation results in larger contact area than the elastic Hertz solution. Therefore, equation (1) is the lower limit of overall contact area.

The upper limit of contact area can be derived based on volume conservation. The volume of the hemisphere before contact is

$$V_1 = \frac{2}{3} \pi R^3 \tag{3}$$

When the interference is close to hemisphere radius, the whole hemisphere deforms plastically. And the hemisphere, either with deformable base or with rigid base, is collapsed, as shown in Figure 2. Since the top contact area is close to the base area, it is reasonable to assume the collapsed hemisphere to be a cylinder with height $R-\omega$ and base area A_u. The volume of the cylinder is

$$V_2 = A_u (R-\omega) \tag{4}$$

Based on volume conservation, the contact area of the collapsed hemisphere is

$$A_u = \frac{2\pi R^3}{3(R-\omega)} \tag{5}$$

As the collapsed hemisphere can never be a cylinder unless the interference reaches hemisphere radius, the contact area with cylinder hypothesis is the upper limit of overall contact area.

The overall contact area of a hemisphere and a rigid plane is bounded by the two limits. At initial contact stage, contact area varies according to Hertz solution. In elastic–plastic contact, the contact area gradually deviates from Hertz solution, and approaches the upper limit for fully plastic contact.

Elastic–plastic contact

Elastic–plastic contact is an important stage in overall contact. The critical interference, which indicates the

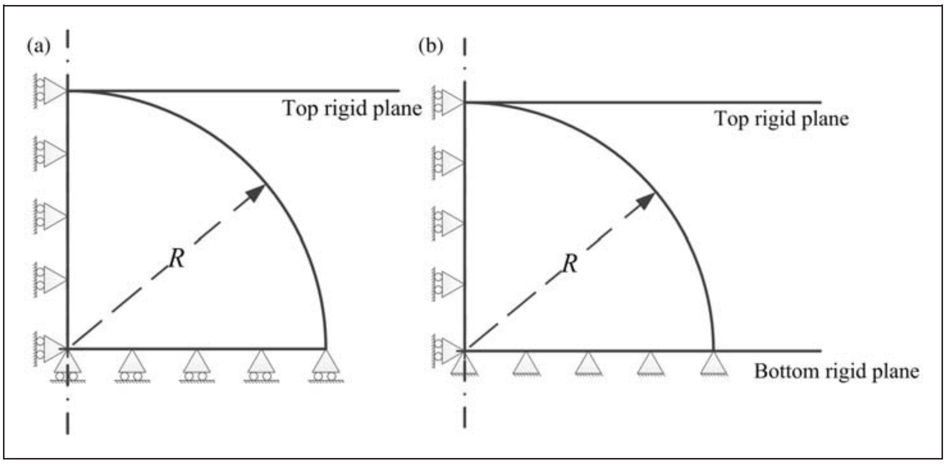

Figure 1. Two cases of the contact of a hemisphere against a rigid flat: (a) deformable base case and (b) rigid base case with additional bottom rigid plane.

onset of plastic deformation in hemisphere, has been formulated in many works.[4,8,16] The critical interferences predicted by these formulations are very close. The analytical formulation derived by Brizmer et al.[16] will be applied in this study

$$\omega_c = \left(\frac{\pi C_\nu Y}{2E'}\right)^2 R \tag{6}$$

where C_ν is the coefficient depends on Poisson's ratio $C_\nu = 1.234 + 1.256\nu$.

In modeling the contact between a hemisphere and a rigid plane, the interference is generally standardized by the critical interference ω_c. As the critical interference depends on material properties ratio e_y, it is not convenient to compare the contact behaviors of different material properties ratios. In order to study the influence of material properties ratio e_y on contact behavior directly, the dimensionless contact interference is defined as

$$\omega^* = \frac{\omega}{R} \tag{7}$$

The contact area and contract load are normalized as

$$A^* = \frac{A}{\pi R^2} \tag{8}$$

$$F^* = \frac{F}{\pi Y R^2} \tag{9}$$

The model proposed by Jackson and Green[8] predicts the early stage elastic–plastic contact behavior well. According to JG model, Hertz solution is still valid at the initial stage of elastic–plastic contact, and the elastic–plastic formulation begins at the interference $1.9\omega_c$. The dimensionless elastic–plastic contact area of JG model is

$$A^* = 1.9^{-Ce_y}\omega^*\left(\frac{\omega^*}{\omega_c^*}\right)^{Ce_y} \tag{10}$$

Also, the dimensionless contact load of JG model is

$$F^* = \frac{4(\omega_c^*)^{\frac{2}{3}}}{3\pi e_y(1-\nu^2)}\left\{\left(\frac{\omega^*}{\omega_c^*}\right)^{\frac{3}{2}}\exp\left(-\frac{1}{4}\left(\frac{\omega^*}{\omega_c^*}\right)^{\frac{5}{12}}\right) + \frac{4H_G}{C_\nu Y}\left[1-\exp\left(-\frac{1}{25}\right)\left(\frac{\omega^*}{\omega_c^*}\right)^{\frac{5}{9}}\right]\left(\frac{\omega^*}{\omega_c^*}\right)\right\} \tag{11}$$

Ce_y and C_ν depend on material properties, $Ce_y = 0.14\exp(23e_y)$ and $C_\nu = 1.295\exp(0.736\nu)$. Here, e_y is material yield stress, Y, to Young's modulus, E, ratio Y/E. According to JG model, H_G/Y is the limit of mean contact pressure to yield stress ratio, which depends on material properties

$$\frac{H_G}{Y} = 2.84\left[1-\exp\left(-0.82\left(\frac{\pi Ce_y}{2}\left(\frac{\omega^*}{\omega_c^*}\right)^{\frac{1}{2}} \times \left(\frac{\omega^*}{1.9\omega_c^*}\right)^{\frac{Ce_y}{2}}\right)^{-0.7}\right)\right] \tag{12}$$

Finite element model

The contact was modeled and analyzed in the commercial ABAQUS package. The top contact rigid flat and added bottom rigid plane were modeled as analytical rigid plane in ABAQUS. The geometric and material properties of the hemisphere were listed in Table 1. As the dimensionless contact behaviors

Table 1. Geometric and material properties of the hemisphere in finite element study.

Property	Value
Radius (mm)	1
Elasticity modulus (GPa)	200
Poisson's ratio	0.2
Yield stress (MPa)	200, 600, 800, 1000, 1600, 2000

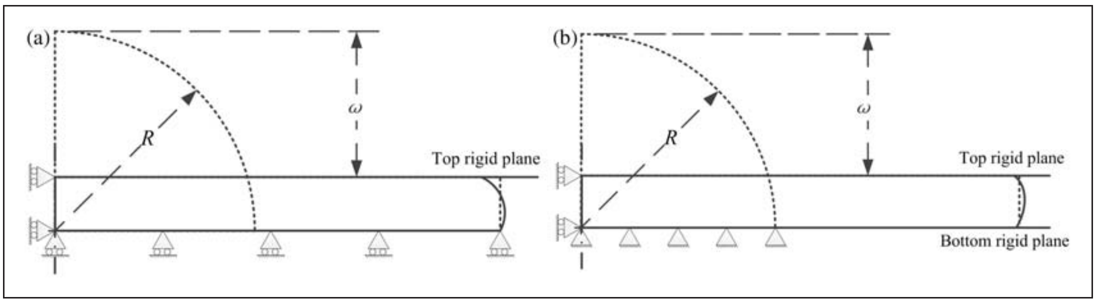

Figure 2. Schematic of the collapse of hemisphere: (a) deformable base case and (b) rigid base case.

were independent of hemisphere radius,[13] the radius of hemisphere was set as 1 mm in finite element analysis. The material of hemisphere was assumed to be elastic perfect plastic. In order to study the influence of material properties ratio on elastic–plastic and plastic contact behaviors, a series of yield stresses ranging from 200 to 2000 MPa were analyzed. As elasticity modulus is kept constant as 200 GPa, the yield stress to elasticity modulus ratio e_y ranged from 0.001 to 0.01. Poisson's ratio had significant influence on early evolution of plastic deformation, while it had little influence on the dimensionless contact area and contact load.[15] A series of Poisson's values ranging from 0.2 to 0.4 were checked in finite element analysis. When the interference is less than $0.1R$, the dimensionless contact area and contact load only increased about 8% as Poisson's ratio changing from 0.2 to 0.4. For larger interferences, the Poisson's ratio almost has no effect on contact area and contact load. Therefore, Poisson's ratio was set as 0.2 in finite element study.

The finite element models established in ABAQUS are shown in Figure 3. The nodes on the symmetry axis of hemisphere were constrained in radial direction. The axial movement of the nodes on hemisphere bottom base was restrained, while the radial movement was not constrained in deformable base case, as illustrated in Figure 3(a). In rigid base case, both axial and radial movements of hemisphere bottom base were restrained. As shown in Figure 3(b), a rigid plane was added at the bottom base. The contact was modeled by surface-to-surface contact in ABAQUS, and the node to surface discretization method was applied. The tangential behavior of the contact was assumed frictionless. In finite element analysis, the displacement was applied at top rigid plane and contact behavior could be obtained from finite element results.

The hemisphere was meshed with 6887 elements, as shown in Figure 3. The four-node linear axisymmetric element CAX4R and three-node linear axisymmetric element CAX3 in ABAQUS were applied. To validate the finite element model, the results were compared with Hertz solution for elastic contact. The finite element model with yield stress 2000 MPa differed from Hertz solution by 3.234% for contact area and 0.5887% for contact load. To validate the

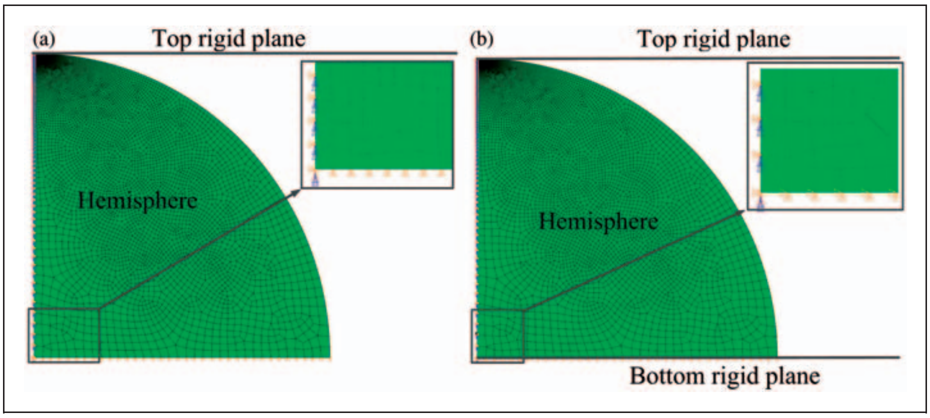

Figure 3. Finite element models for the contact of a hemisphere against a rigid plane: (a) deformable base case and (b) rigid base with additional bottom rigid plane.

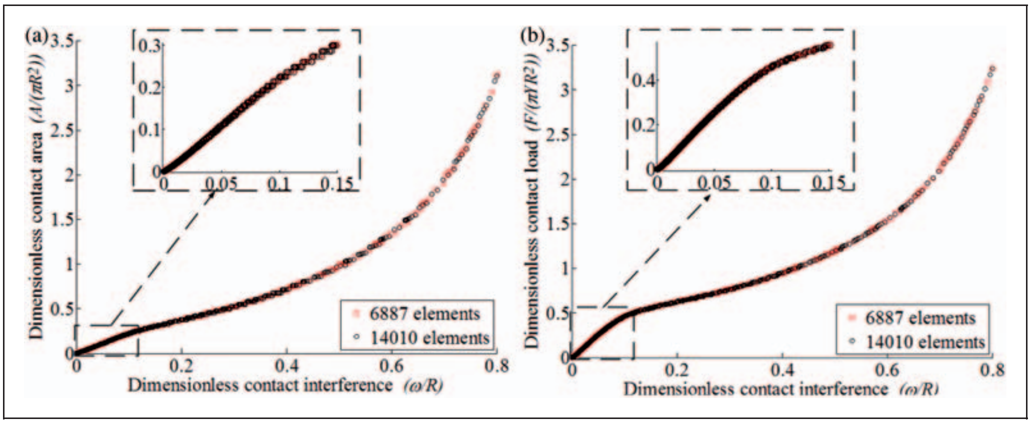

Figure 4. Comparisons of finite element results of different mesh densities under deformable base condition with material $e_y = 0.005$: (a) the comparison of contact areas and (b) the comparison of contact loads.

mesh density, this model was compared with a double meshed model, which consisted of 14,010 elements. For deformable base case, contact areas and contact loads of different mesh densities were compared in Figure 4(a) and (b), respectively. For rigid base case, the comparisons were given in Figure 5(a) and (b).

As shown in Figures 4 and 5, the contact areas and contact loads of the models with different mesh densities were difficult to discriminate. Therefore, the hemisphere was mashed with 6887 elements in this study.

Results and discussion

With the increase of contact interference, the hemisphere would gradually deform elastically, elastic–plastically, and finally plastically. The evolution of stresses has been investigated in the literatures,[8,13] and it will not be analyzed here. This study focus on contact area, mean contact pressure, and contact load of the overall contact between a hemisphere and a rigid flat.

Overall contact behavior

The overall contact areas of finite element model with yield stress 1000 MPa are plotted in Figure 6. The cases of deformable and rigid bases are given in Figure 6(a) and (b), respectively. The contact area coincides with Hertz solution for small contact interferences. With the increase of interference, contact area increases faster than Hertz solution. The difference between contact area and Hertz solution grows with the increase of interference. When the interference is close to the radius of hemisphere, contact area gradually approaches the upper limit. The overall contact area varies between Hertz solution and the upper limit. The dimensionless contact area reaches 1 when the interference is about 0.5. This coincides with AF model,[7] while contact area does not vary linearly, especially for deformable base case. For different base conditions, the variations of contact areas are different, especially for large interferences. The differences of the two cases will be discussed later.

The overall mean contact pressure can be derived from contact area and contact load. The overall mean contact pressures of deformable and rigid base cases are given in Figure 7(a) and (b). It can be seen that the mean contact pressure increases rapidly for small interferences. The mean contact pressure reaches maximum value for certain interference and decreases gradually with the increase of interference. For the material with yield stress 1000 MPa, the maximum

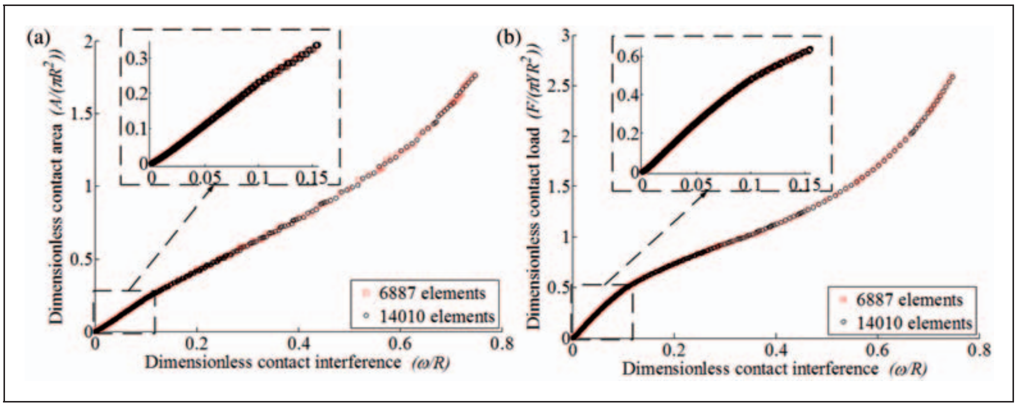

Figure 5. Comparisons of finite element results of different mesh densities under rigid base condition with material $e_y = 0.005$: (a) the comparison of contact areas and (b) the comparison of contact loads.

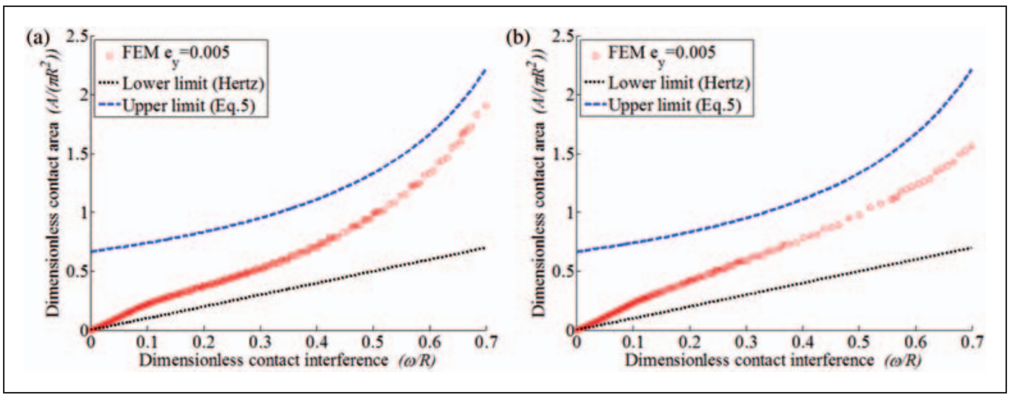

Figure 6. The overall contact areas of finite element results: (a) deformable base case and (b) rigid base case.

dimensionless mean contact pressure is about 2.5 and happens when the dimensionless interference is about 0.02. The maximum mean contact pressure and the corresponding interference relate to material properties ratio. After passing maximum value, the mean contact pressure gradually decreases to a constant value when the interference approaches the hemisphere radius.

Figure 8 shows the overall contact loads of the finite model with yield stress 1000 MPa. The contact loads of deformable and rigid bases are plotted in Figure 8(a) and (b), respectively. The contact load increases rapidly when the interference is less than 0.1. The increase slows down when the interference is greater than 0.1, while contact load increases more and more rapidly with the increase of interference. The variation of contact load relates to the variations of contact area and mean contact pressure. For interferences less than 0.1, although mean contact pressure reaches its maximum and then decreases to some degree, contact area keeps increasing. As a result, contact load increases rapidly. For interferences larger than 0.1, mean contact pressure keeps decreasing, and the increase of contact area slows down. Therefore, it is obvious that the increase of contact load slows down. When the interference is greater than 0.5, mean contact pressure gradually decreases to a constant value, therefore, the variation of contact load is similar to contact area.

Influence of material properties ratio

A series of material yield stress Y are studied to investigate the influence of material properties ratio e_y. The contact areas, mean contact pressures, and contact loads of finite element models with yield stresses 200, 1000, and 2000 MPa are compared. As elasticity modulus is held constant as 200 GPa in this study, the material properties ratios of the finite element models are 0.001, 0.05, and 0.01, respectively.

For deformable base case, the contact areas with different material properties ratios are compared in Figure 9. For elastic contact, material properties ratio e_y has no influence on contact area according to Hertz solution. As shown in Figure 9(a), with the increase of interference, the contact areas gradually deviate from Hertz solution. Since the critical interference of smaller material properties ratio is smaller, plastic deformation occurs earlier in the hemisphere and the contact area deviates from

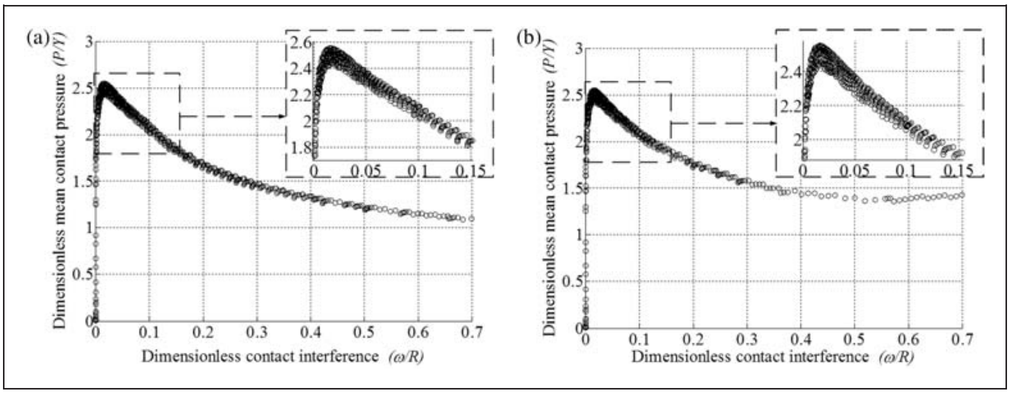

Figure 7. The overall mean contact pressures of the finite element results with $e_y = 0.005$: (a) the mean contact pressure of deformable base and (b) the mean contact pressure of rigid base.

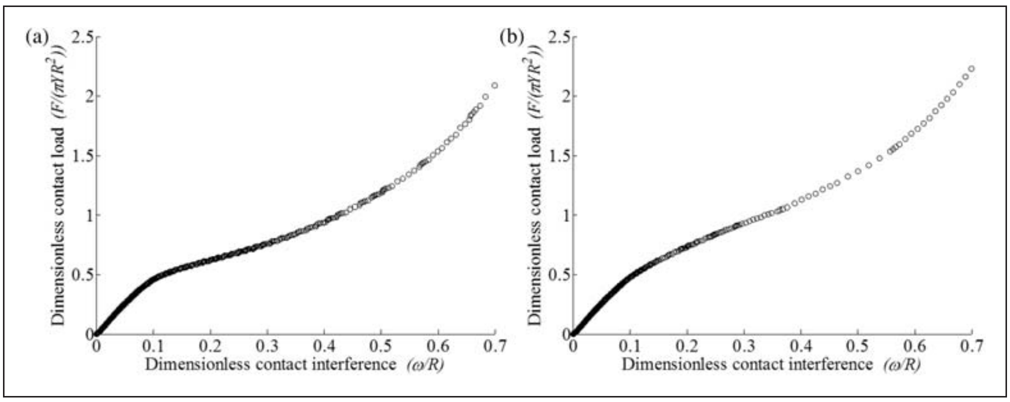

Figure 8. The overall contact loads of finite element model with $e_y = 0.005$: (a) contact load of deformable base case and (b) contact load of rigid base case.

Hertz solution earlier. As a result, the contact area of smaller material properties ratio is larger. With the interference increasing to 0.5, the differences of the contact areas of different material properties ratios gradually reduce, as illustrated in Figure 9(b). For contact interferences larger than 0.5, the contact areas are not affected by material properties ratio. This is because for large interferences, all the contacts with different material properties ratios become fully plastic, which is independent of material properties ratio. For rigid base case, the contact areas of different material properties ratios are given in Figure 10. The influence of material properties ratio on the contact area of rigid base is similar to deformable base case.

It can be seen that material properties ratio has no influence on elastic contact area. With interference increasing to 0.5, the influence of material properties ratio becomes more and more obvious at first and then gradually fades. When the interference is larger than 0.5, material properties ratio has no effect on contact area.

As shown in Figure 11, the mean contact pressures of different material properties ratios are compared. Comparison of the mean contact pressures under deformable base condition is shown in Figure 11(a). It is obvious that the maximums of mean contact pressure and the corresponding interferences vary with material properties ratios. The smaller material properties ratio will lead to larger maximum mean contact pressure and smaller corresponding interference. It is interesting that the maximum mean contact pressure of material properties ratio $e_y = 0.001$ is close to 2.8, which coincides with the results of Jackson and Green.[8] With the increase of interference, the influence of material properties ratio gradually fades. When the interference is greater than 0.5, the mean contact pressures of different material properties ratios are very close. The comparison of mean contact pressures of rigid base is similar to deformable base case, as shown in Figure 11(b).

The contact loads of different material properties ratios are shown in Figure 12. The cases of deformable and rigid bases are compared in Figure 12(a) and (b), respectively. Similar to the influence on contact area, contact load is not affected by material properties ratio for elastic contact. When the interference is less than 0.5, the influence of material properties ratio on contact load is obvious, especially for the interferences about 0.1. The contact load of smaller material properties ratio is larger. When the interference

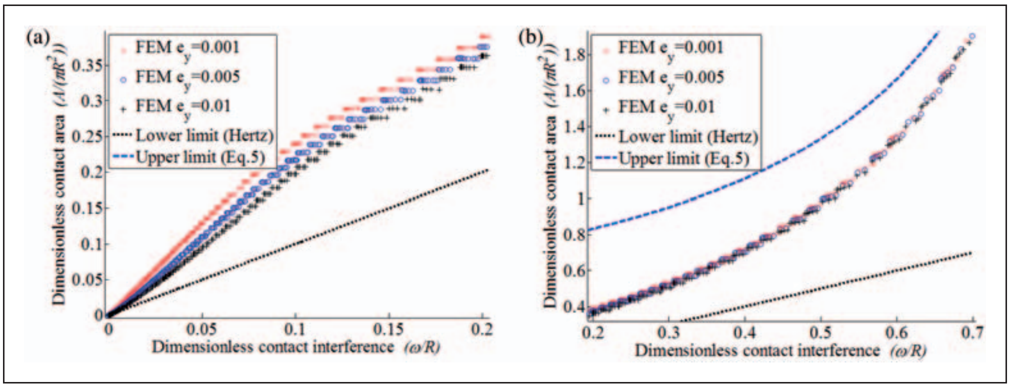

Figure 9. Comparison of contact areas with different material properties ratios for deformable base case: (a) the comparison in interference range $0 < \omega^* < 0.2$ and (b) the comparison in interference range $0.2 < \omega^* < 0.7$.

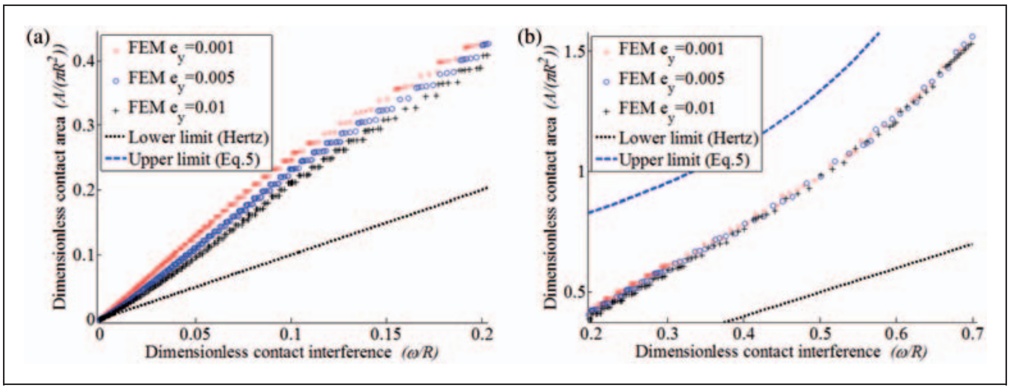

Figure 10. Comparison of contact areas with different material properties ratios for rigid base case: (a) the comparison in interference range $0 < \omega^* < 0.2$ and (b) the comparison in interference range $0.2 < \omega^* < 0.7$.

increases to 0.5, the influence gradually fades. For interferences larger than 0.5, material properties ratio has no influence on contact load. For rigid base case, the influence of material properties ratio on contact load is similar to deformable base case, as shown in Figure 12(b).

From the comparisons of contact areas, mean contact pressures, and contact loads of different material properties ratios, it can be seen that material properties ratio has no influence on elastic contact, while it affects elastic–plastic and plastic contact behaviors much when the interference is less than 0.5, especially for the interferences about 0.1. When the interference is larger than 0.5, material properties ratio does not affect the contact behaviors.

Influence of base boundary condition

In order to study the influence of radial movement of hemisphere base on overall contact behavior, the contact areas, mean contact pressures, and contact loads of radial deformable and radial rigid base cases are compared, respectively.

As shown in Figure 13, the overall contact areas of deformable and rigid bases are plotted and compared. According to Saint Venant's principle, the influence of base boundary condition can be neglected when the interference is less than 0.1 and the contact areas of deformable and rigid bases are very close. With the increase of interference, the difference between the contact areas of deformable and rigid bases is apparent. For the interferences in the range $0.1 < \omega^* < 0.5$, the contact area of rigid base is larger than deformable base case. When the interference is greater than 0.5, the contact area of deformable base case gradually becomes larger than rigid base case. In this stage, the contact area of deformable base case is more close to the upper limit.

Comparison of the mean contact pressures of deformable and rigid bases is given in Figure 14. The mean contact pressures are almost the same for interferences less than 0.1. For larger interferences, the difference becomes apparent. The mean contact pressure of deformable base decreases faster than rigid base case. With the increase of interference, the mean contact pressure gradually decreases to 1 for

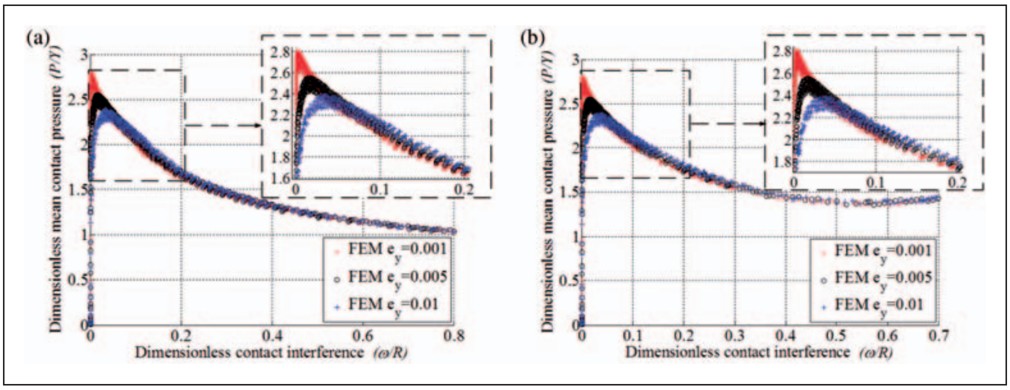

Figure 11. Comparison of mean contact pressures with $e_y = 0.001$, $e_y = 0.005$, and $e_y = 0.01$: (a) comparison of mean contact pressures for deformable base case and (b) comparison of mean contact pressures for rigid base case.

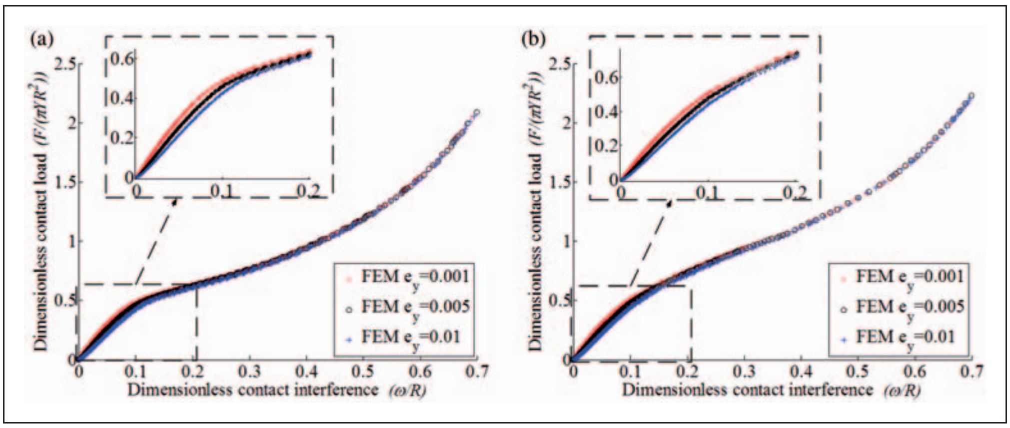

Figure 12. Comparison of contact loads with $e_y = 0.001$, $e_y = 0.005$, and $e_y = 0.01$: (a) comparison of contact loads for deformable base case and (b) comparison of contact loads for rigid base case.

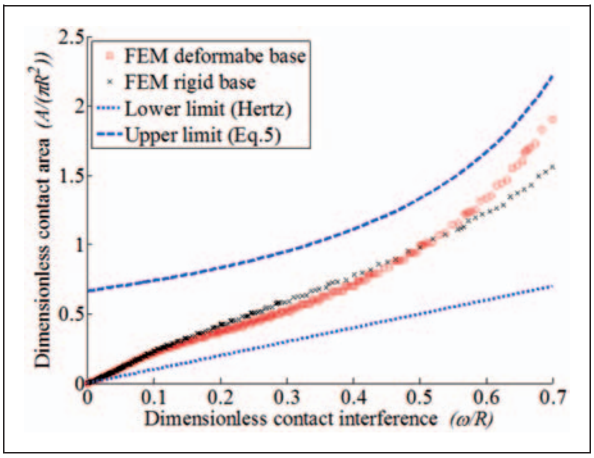

Figure 13. Comparison of contact areas of deformable and rigid bases with $e_y = 0.005$.

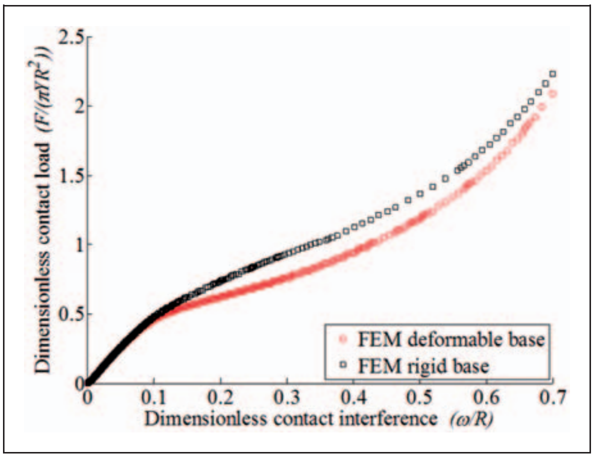

Figure 15. Comparison of contact loads of deformable and rigid bases with $e_y = 0.005$.

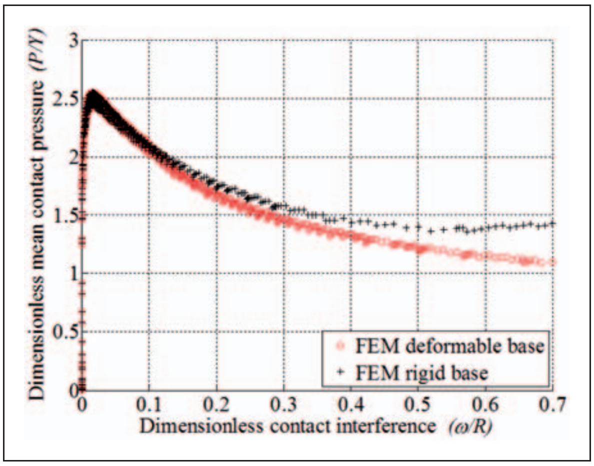

Figure 14. Comparison of mean contact pressures of deformable and rigid bases with $e_y = 0.005$.

deformable base case, while it decreases to the value about 1.4 for rigid base case.

Comparison of the contact loads of deformable and rigid base cases is shown in Figure 15. According to Saint Venant's principle, the base boundary condition has little influence on contact load when the interference is less than 0.1. With the increase of interference, the contact load of rigid base case becomes larger than deformable base case. The difference between the contact loads increases when the interference is in the range $0.1 < \omega^* < 0.4$ and then gradually decrease with the increase of interference.

Comparisons of contact areas, mean contact pressures, and contact loads of the deformable and rigid base cases show that, the base boundary condition has little influence on the contact behaviors when interference is less than 0.1. For larger interferences, contact areas, mean contact pressures, and contact loads are quite different for different base boundary conditions. Therefore, the contact behaviors of deformable and rigid bases should be modeled separately.

Empirical formulation of overall contact behavior

The overall contact behavior can be formulated by empirical expressions. Contact area and contact load, which are the main concerns of contact behaviors, will be formulated based on some existing models and finite element results. The contact behaviors of deformable and rigid bases will be formulated separately.

JG model coincides with finite element results well for small interferences and it will be applied to model the contact behaviors of early stage. Finite element analysis show that JG model is valid when the interference is less than $0.6528\omega_c^*/e_y$. For interferences larger than $0.6528\omega_c^*/e_y$, the contact behaviors will be formulated by fitting finite element results.

Contact interference, contact area, and contact load are normalized according to equations (7) to (9), respectively. Therefore, the formulations of contact area and contact load are general solutions for the contact of a hemisphere against a rigid flat.

Deformable base case. For deformable base case, elastic contact and early elastic–plastic contact can be modeled by Hertz solution and JG model, respectively. For interferences beyond the valid range of JG model, the contact range can be divided into three stages according to the influence of material properties ratio. For interferences in the stage $0.6528\omega_c^*/e_y \leqslant \omega^* < 0.118$, the influence of material properties ratio e_y becomes more and more apparent. For the stage $0.118 \leqslant \omega^* < 0.5$, the influence of e_y gradually fades. Material properties ratio e_y does not affect the contact behaviors for the stage $0.5 \leqslant \omega^* < 1$. Contact areas and contact loads for the three stages can be formulated by fitting finite element results.

The overall contact area for deformable base case is formulated as equation (13). The first two parts of

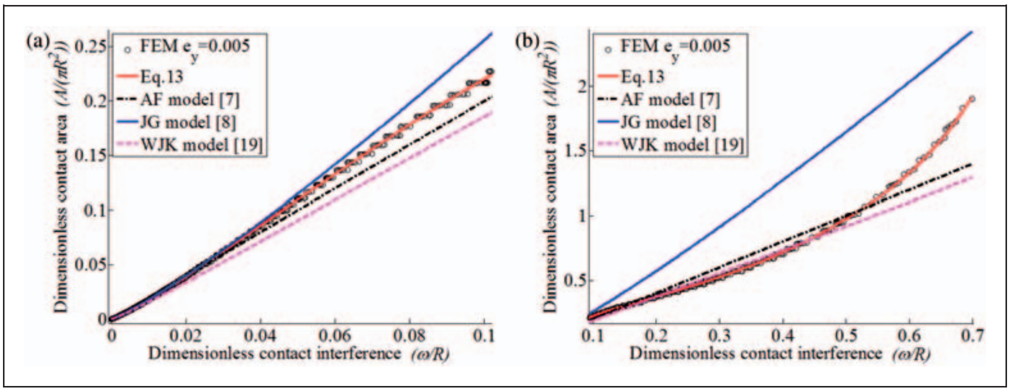

Figure 16. Comparison of the contact areas for deformable base case: (a) comparison in interference range $0 < \omega^* < 0.1$ and (b) comparison in interference range $0.1 < \omega^* < 0.7$.

equation (13) are from Hertz solution and JG model, respectively. While the last three parts of equation (13) relate to the three stages beyond the valid range of JG model. The influence of material properties ratio e_y is considered in the coefficients $C_{Ad1} - C_{Ad8}$

$$\begin{array}{lll} A_d^* = \omega^* & \text{for} & 0 < \omega^* \leqslant 1.9\omega_c^* \\ A_d^* = 1.9^{-C_{e_y}}\omega^*\left(\omega^*/\omega_c^*\right)^{C_{e_y}} & \text{for} & 1.9\omega_c^* < \omega^* \leqslant 0.6528\omega_c^*/e_y \\ A_d^* = \left(C_{Ad1}\omega^{*3} + C_{Ad2}\omega^{*2} + C_{Ad3}\omega^* + C_{Ad4}\right)/\pi & \text{for} & 0.6528\omega_c^*/e_y < \omega^* \leqslant 0.118 \\ A_d^* = \left(C_{Ad5}\omega^{*3} + C_{Ad6}\omega^{*2} + C_{Ad7}\omega^* + C_{Ad8}\right)/\pi & \text{for} & 0.118 < \omega^* \leqslant 0.5 \\ A_d^* = 2R(C_{Ad9}\omega^* + C_{Ad10})/(3(1-\omega^*)) & \text{for} & 0.5 \leqslant \omega^* < 0.75 \end{array} \quad (13)$$

The coefficients in equation (13) are

$$C_{Ad1} = -131.9;\ C_{Ad2} = 136.2e_y^{0.3171} - 7.911;$$

$$C_{Ad3} = -45.99e_y^{0.5321} + 9.351;$$

$$C_{Ad4} = 295.1e_y^2 - 4.818e_y - 0.0003371;$$

$$C_{Ad5} = 16.43;\ C_{Ad6} = -8.6186;$$

$$C_{Ad7} = -0.07909e_y^{-0.2287} + 6.249;$$

$$C_{Ad8} = -1.492e_y^{0.4413} + 0.3261;$$

$$C_{Ad9} = 0.6665;\ C_{Ad10} = 0.3989$$

Figure 16 shows the comparison of equation (13), finite element results, and some existing models. As illustrated in Figure 16(a), all models are close to finite element results for small interferences. With the increase of interference, the difference between the existing models and finite element results gradually appears. JG model overestimates contact area, while AF and Wadwalkar, Jackson, and Kogut (WJK) models underestimate contact area. As shown in Figure 16(b), for larger interferences, the difference between JG model and finite element results is apparent. The contact area of AF model is greater than finite element results for the interferences in the range $0.2 < \omega^* < 0.5$, while AF mode underestimates the contact area for interferences greater than 0.5. The contact area of WJK model is close to finite element results in the range $0.2 < \omega^* < 0.5$ and then it becomes less than finite element results when the interference is larger than 0.5. By adopting JG model and fitting finite element results, equation (13) fits finite element results well in overall contact range and it could model the contact area of deformable base case more accurately.

The contact load of deformable base is formulated as equation (14). The first two parts of equation (14) are from Hertz solution and JG model, respectively. And the last three parts, which relate to the three stages beyond the valid range of JG model, are obtained by fitting finite element results. The influence of material properties ratio is represented in the coefficients $C_{Fd1} - C_{Fd8}$

$$\begin{array}{lll} F_d^* = \dfrac{4(\omega^*)^{\frac{3}{2}}}{3\pi e_y(1-\nu^2)} & \text{for} & 0 < \omega^* \leqslant 1.9\omega_c^* \\ F_d^* = \dfrac{4(\omega_c^*)^{\frac{3}{2}}}{3\pi e_y(1-\nu^2)}\left\{\begin{array}{l}\left[\exp\left(-\dfrac{1}{4}\left(\dfrac{\omega^*}{\omega_c^*}\right)^{\frac{5}{12}}\right)\right]\left(\dfrac{\omega^*}{\omega_c^*}\right)^{\frac{3}{2}} \\ +\dfrac{4H_G}{C_\nu Y}\left[1-\exp\left(-\dfrac{1}{25}\right)\left(\dfrac{\omega^*}{\omega_c^*}\right)^{\frac{5}{9}}\right]\left(\dfrac{\omega^*}{\omega_c^*}\right)\end{array}\right\} & \text{for} & 1.9\omega_c^* \leqslant \omega^* \leqslant 0.6528\omega^*/e_y \\ F_d^* = C_{Ld1}\omega^{*3} + C_{Ld2}\omega^{*2} + C_{Ld3}\omega^* + C_{Ld4} & \text{for} & 0.6528\omega_c^*/e_y \leqslant \omega^* \leqslant 0.118 \\ F_d^* = C_{Ld5}\omega^{*3} + C_{Ld6}\omega^{*2} + C_{Ld7}\omega^* + C_{Ld8} & \text{for} & 0.118 \leqslant \omega^* \leqslant 0.5 \\ F_d^* = C_{Ld9}\omega^{*3} + C_{Ld10}\omega^{*2} + C_{Ld11}\omega^* + C_{Ld12} & \text{for} & 0.5 \leqslant \omega^* \leqslant 0.75 \end{array} \quad (14)$$

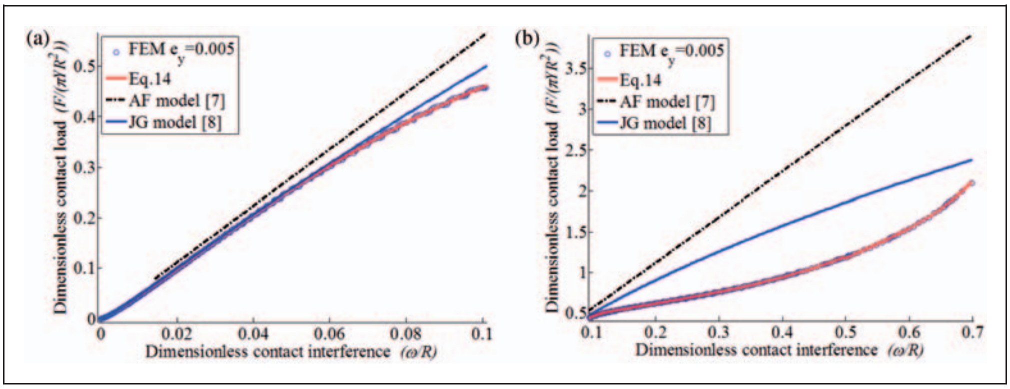

Figure 17. Comparison of the contact loads for deformable base case: (a) comparison in interference range $0 < \omega^* < 0.1$ and (b) comparison in interference range $0.1 < \omega^* < 0.7$.

The coefficients in equation (14) are

$$C_{Fd1} = -1628 e_y^{0.666} - 19.66;$$
$$C_{Fd2} = 503 e_y^{0.5716} - 26.8$$
$$C_{Fd3} = -81.5 e_y^{0.7091} + 7.564;$$
$$C_{Fd4} = -2.128 e_y^3 + 603.3 e_y^2 - 6.201 e_y + 0.003508;$$
$$C_{Fd5} = 94.89 e_y + 5.389; \; C_{Fd6} = -119.3 e_y - 2.821;$$
$$C_{Fd7} = 37.49 e_y^{0.933} + 1.758;$$
$$C_{Fd8} = -4.744 e_y^{0.8471} + 0.3585;$$
$$C_{Fd9} = 55.523; \; C_{Fd10} = -89.661;$$
$$C_{Fd11} = 51.807; \; C_{Fd12} = -9.2539$$

$0.6528\omega_c^*/e_y \leqslant \omega^* < 0.1$, the influence of material properties ratio becomes more and more obvious. For interferences in the range $0.1 \leqslant \omega^* < 0.5$, the influence of material properties ratio gradually fades. When the interference is in the range $0.5 \leqslant \omega^* < 1$, contact behaviors are almost not affected by material properties ratio e_y, and contact areas and contact loads can be formulated by fitting finite element results.

The overall contact area of rigid base are formulated in equation (15). The first two parts of equation (15) are from Hertz solution and JG model, respectively. While the last three parts of equation (15) correspond to the stages beyond the valid range of JG model. The influence of material properties ratio e_y is considered in the coefficients $C_{Ar1} - C_{Ar6}$

$$\begin{array}{lll} A_r^* = \omega^* & \text{for} & 0 < \omega^* \leqslant 1.9\omega_c^* \\ A_r^* = 1.9^{-Ce_y} \omega^* \left(\omega^*/\omega_c^*\right)^{Ce_y} & \text{for} & 1.9\omega_c^* < \omega^* \leqslant 0.6528\omega_c^*/e_y \\ A_r^* = \left(C_{Ar1}\omega^{*3} + C_{Ar2}\omega^{*2} + C_{Ar3}\omega^* + C_{Ar4}\right)/\pi & \text{for} & 0.6528\omega_c^*/e_y \leqslant \omega^* \leqslant 0.1 \\ A_r^* = \left(C_{Ar5}\omega^* + C_{Ar6}\right)/\pi & \text{for} & 0.1 < \omega^* \leqslant 0.5 \\ A_r^* = \left(C_{Ar7}\omega^{*3.474} + C_{Ar8}\right)/\pi & \text{for} & 0.5 \leqslant \omega^* < 0.75 \end{array} \qquad (15)$$

The contact loads of finite element results, JG model, AF model, and equation (14) are compared in Figure 17. The JG model coincides with finite element results well at early stage of contact, while it gradually overestimates contact load with the increase of interference. The AF model predicts larger contact load than finite element model in the overall range. It is obvious that equation (14) fits the finite element results well in the overall range, and it can be used to model the overall contact load for deformable base case.

Rigid base case. The contact area and contact load of rigid base case can be formulated by the same way as deformable base case. The elastic contact and early elastic–plastic contact are modeled by Hertz solution and JG model. For the interferences beyond the valid range of JG model, the division of the stages is slightly different from deformable base case. For the stage

The coefficients in equation (15) are as follows

$$C_{Ar1} = -62.66; \; C_{Ar2} = 282.5 e_y^{0.566} - 2.497;$$
$$C_{Ar3} = -104.2 e_y^{0.7489} + 8.807;$$
$$C_{Ar4} = 550.4 e_y^2 - 7.17 e_y + 0.002895;$$
$$C_{Ar5} = 17.63 e_y + 5.66;$$
$$C_{Ar6} = 357.7 e_y^2 - 20.39 e_y + 0.2455;$$
$$C_{Ar7} = 9.003; \; C_{Ar8} = 2.339$$

As shown in Figure 18, the contact areas of different models are compared with the finite element results of rigid base case. It can be seen from Figure 18(a) that all models are consistent with finite element results when the interference is less than 0.04. With the increase of interference, JG model gradually overestimates contact area. AF model underestimates contact area

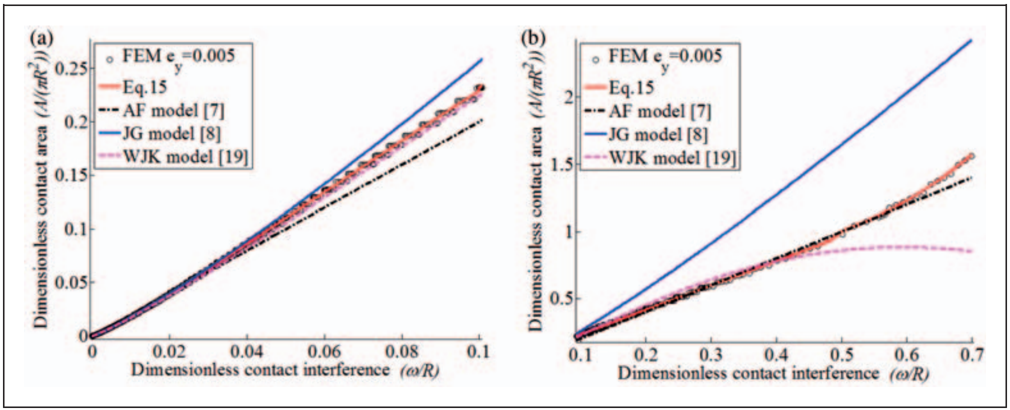

Figure 18. Comparison of the contact areas for rigid base case: (a) comparison in interference range $0 < \omega^* < 0.1$ and (b) comparison in interference range $0 < \omega^* < 0.7$.

when the interference is about 0.1, while it is close to the finite element results for the interferences in $0.2 < \omega^* < 0.5$, as shown in Figure 18(b). WJK model fits finite element results well for the interferences within 0.55, while it deviates from finite element results for larger interferences. It can be seen that equation (15) coincides with finite element results well in the overall range

$$
\begin{aligned}
&F_r^* = \frac{4(\omega^*)^{\frac{3}{2}}}{3\pi e_y(1-\nu^2)} && \text{for} \quad 0 < \omega^* \leqslant 1.9\omega_c^* \\
&F_r^* = \frac{4(\omega_c^*)^{\frac{3}{2}}}{3\pi e_y(1-\nu^2)} \left\{ \begin{array}{l} \left[\exp\left(-\frac{1}{4}\left(\frac{\omega^*}{\omega_c^*}\right)^{\frac{5}{12}}\right)\right]\left(\frac{\omega^*}{\omega_c^*}\right)^{\frac{3}{2}} \\ +\frac{4H_G}{C_\nu Y}\left[1-\exp\left(-\frac{1}{25}\right)\left(\frac{\omega^*}{\omega_c^*}\right)^{\frac{5}{9}}\right]\left(\frac{\omega^*}{\omega_c^*}\right) \end{array} \right\} && \text{for} \quad 1.9\omega_c^* < \omega^* \leqslant_c 0.6528\omega^*/e_y \\
&F_r^* = C_{Lr1}\omega^{*3} + C_{Lr2}\omega^{*2} + C_{Lr3}\omega^* + C_{Lr4} && \text{for} \quad 0.6528\omega_c^*/e_y < \omega^* \leqslant 0.1 \\
&F_r^* = C_{Lr5}\omega^{*3} + C_{Lr6}\omega^{*2} + C_{Lr7}\omega^* + C_{Lr8} && \text{for} \quad 0.118 < \omega^* \leqslant 0.5 \\
&F_r^* = C_{Lr9}\omega^{*3} + C_{Lr10}\omega^{*2} + C_{Lr11}\omega^* + C_{Lr12} && \text{for} \quad 0.5 < \omega^* \leqslant 0.75
\end{aligned} \tag{16}
$$

The coefficients in equation (16) are as follows

$$
\begin{aligned}
C_{Fr1} &= 9.348e_y^{-0.3698} - 78.23; \\
C_{Fr2} &= 179.7e_y^{0.1001} - 114.2; \\
C_{Fr3} &= -24.55e_y^{0.4351} + 8.354; \\
C_{Fr4} &= -0.5627e_y^{0.5983} + 0.00606; \\
C_{Fr5} &= 27.04e_y^{0.3996} + 6.672; \\
C_{Fr6} &= -36.39e_y^{0.5014} - 6.592; \\
C_{Fr7} &= 21.66e_y^{0.6461} + 3.931; \\
C_{Fr8} &= -6.085e_y^{0.7973} + 0.1848; \\
C_{Fr9} &= 22.87; \; C_{Fr10} = -31.621; \\
C_{Fr11} &= 17.34; \; C_{Fr12} = -2.264
\end{aligned}
$$

The contact load of rigid base is formulated as equation (16). The first two parts of equation (16) are from Hertz solution and JG model, respectively. The last three parts of equation (16) are obtained by fitting finite element results. The influence of material properties is considered in the coefficients $C_{Fr1} - C_{Fr8}$.

For rigid base case, the contact loads of different models are compared in Figure 19. It is clear that AF model overestimates contact load in the overall range. JG model is close to finite element results for small contact interferences, as illustrated in Figure 19(a). The difference between JG model and finite element results is obvious for large contact interferences, as shown in Figure 19(b). It can be seen that equation (16) coincides with finite element results well in the overall range. Therefore, equation (16) could model the overall contact load accurately.

By comparing with finite element results and some existing models, it can be seen that equations (13) and (14) could predict the overall contact area and contact load of deformable base case accurately. The contact area and contact load of rigid base can be modeled by equations (15) and (16) accurately in the overall range.

Comparison with experimental results

Many experimental works for the contact of a hemisphere and a rigid flat have been published. In order to validate this study, the proposed formulations are compared with the experimental results given by Ovcharenko et al.,[17] Jamari and Schipper,[9] and Chaudhri et al.[11]

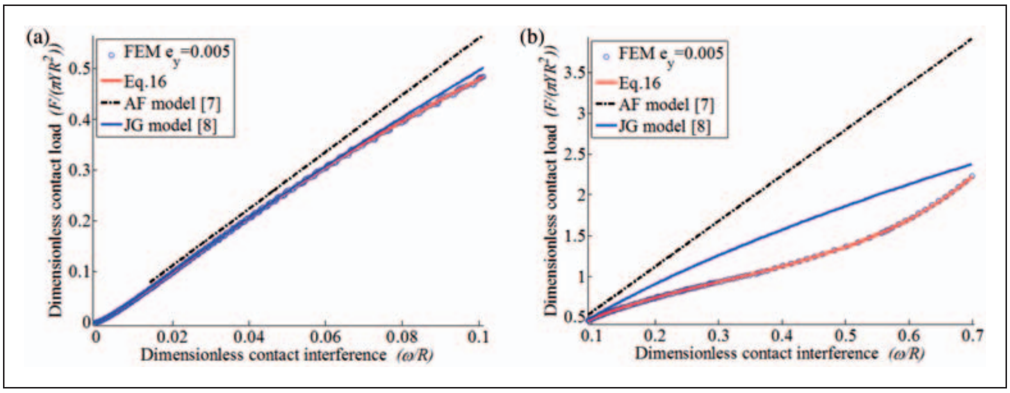

Figure 19. Comparison of the contact loads for rigid base case: (a) comparison in interference range $0 < \omega^* < 0.1$ and (b) comparison in interference range $0.1 < \omega^* < 0.7$.

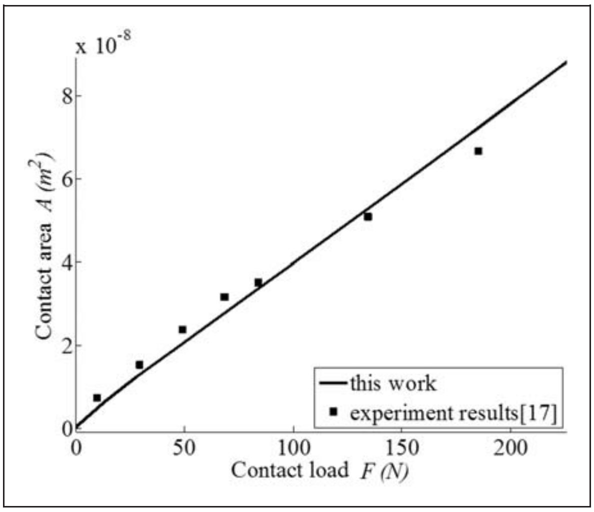

Figure 20. Comparison of this study with experiment results:[16] contact area vs. contact load.

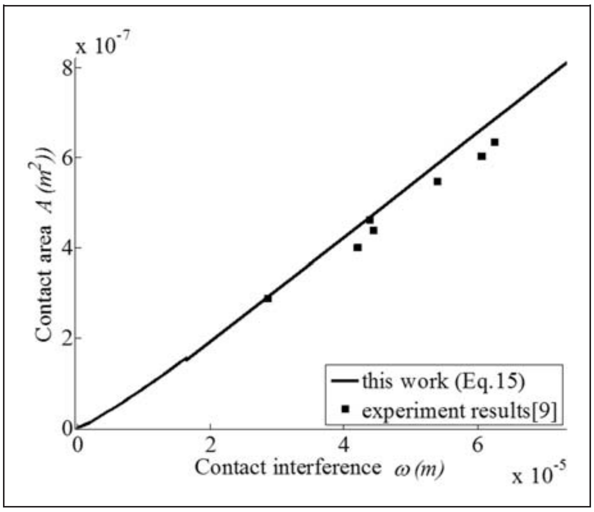

Figure 21. Comparison of this study with experiment results:[9] contact area vs. contact interference.

Ovcharenko et al.[17] measured the contact areas under given contact loads of a stainless steel sphere contacting against a rigid flat. The sphere radius is 1.19 mm. The elasticity modulus of stainless steel is 200 GPa, and the yield stress is 1080 MPa. Poisson's ratio is 0.30. The measured results are compared with the formulations of rigid base case of this study.

As shown in Figure 20, comparison of this study with the experimental results of Ovcharenko et al.[17] is presented. It can be seen that this study coincides with the experiment data well, which validates this study. As the loads of the experiment are relatively small, the contact areas and contact loads all fall in the range of the second part in equations (15) and (16), respectively. Therefore, the comparison is actually between the experimental data and JG model,[8] which is adopted as the section part of the model in this study.

In order to validate the contact stages beyond the valid range of JG model, comparison with the experiment work of Jamari and Schipper[9] is presented. A copper sphere contacting against a rigid flat was measured by Jamari and Schipper.[9] The hardness of the copper in the experiment is 1.2 GPa, the elasticity modulus is 120 GPa, and the Poisson's ratio is 0.35. The sphere diameter is 3 mm.

In the experiment of Jamari and Schipper,[9] the contact load is large enough that the contact is beyond the valid range of JG model. The comparison of equation (15) and the experimental data of Jamari and Schipper[9] is given in Figure 21. It can be seen that equation (15) is slightly larger than the measurements, while it coincides with the experimental results well, which validates the accuracy of the proposed formulations in this study.

Chaudhri et al.[11] measured the mean contact pressure of a phosphor bronze sphere pressed by two rigid flats. The radius of the measured sphere is 1.5875 mm. The material elasticity modulus is 115 GPa, and the Poisson's ratio is 0.35. The hardness is about 2.7 GPa, and the yield stress is about 857 MPa.[19] The experiment cover fully plastic contact and it will be compared with the formulations of deformable base case. In order to compare with the experimental results, the contact radius is derived from equation (13) and the

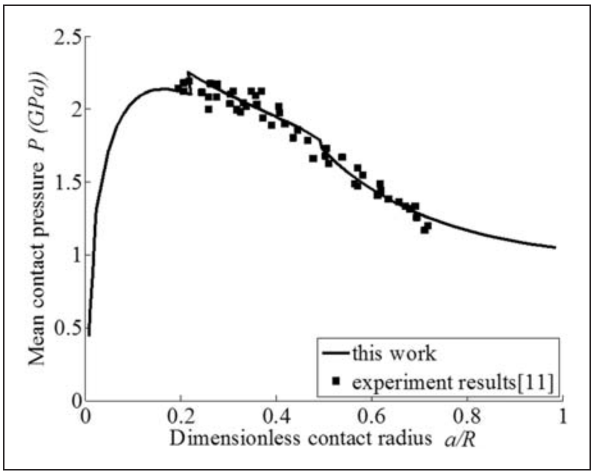

Figure 22. Comparison of this study with experiment results:[11] mean contact pressure vs. dimensionless contact radius.

mean contact pressure is obtained from equations (13) and (14).

Figure 22 shows the comparison of the experimental results[11] with this study. Since the proposed formulations are section wise, there are several jumps in mean contact pressure curve. However, the mean contact pressure predicted by this study fits well with the experimental results.

The comparisons with several experimental results indicate that this study can predict the overall contact behavior of an elastic–plastic sphere and a rigid flat well.

Conclusions

The overall contact of a hemisphere against a rigid plane is studied in this study. The upper limit of overall contact area is derived based on volume conservation. A finite element model on the contact of a hemisphere and a rigid plane is established and analyzed. The influences of material yield stress to elasticity modulus ratio and base boundary condition are investigated. By adopting some existing models and fitting finite element results, empirical formulations for overall contact area and contact load are obtained.

Finite element study shows that the overall contact area is bounded by Hertz solution and the upper limit. The material yield stress to elasticity modulus ratio mainly affects the contact behaviors (contact area, mean contact pressure, and contact load) in the early stage of contact. When the dimensionless interference is larger than 0.5, the material properties ratio has no influence on the contact behaviors. The boundary condition of hemisphere base affects the contact behaviors significantly for large interferences, but the influence can be neglected at early stage of contact.

By comparing with finite element results, some existing models, and experimental data, this study is suitable to model the overall contact area and contact load of an elastic perfectly plastic hemisphere against a rigid plane.

Funding

This work was supported by the 863 project of Ministry of Science and Technology, China (grant no. 2008AA05A302).

Acknowledgment

The authors are grateful for the comments and help of reviewers and editors.

References

1. Greenwood JA and Williamson J. Contact of nominally flat surfaces. *Proc R Soc London Ser A* 1966; 295: 300–319.
2. Kogut L and Etsion I. A finite element based elastic-plastic model for the contact of rough surfaces. *Tribol Trans* 2003; 46: 383–390.
3. Jackson RL and Green I. A statistical model of elasto-plastic asperity contact between rough surfaces. *Tribol Int* 2006; 39: 906–914.
4. Chang WR, Etsion I and Bogy DB. An elastic-plastic model for the contact of rough surfaces. *J Tribol* 1987; 109: 257–263.
5. Majumdar A and Bhushan B. Fractal model of elastic-plastic contact between rough surfaces. *J Tribol* 1991; 113: 1–13.
6. Timoshenko SP and Goodier JN. *Theory of elasticity*. New York: McGraw-Hill, 1970.
7. Abbott EJ and Firestone FA. Specifying surface quality – a method based on accurate measurement and comparison. *Mech Eng (Am Soc Mech Eng)* 1933; 55: 569–572.
8. Jackson RL and Green I. A finite element study of elasto-plastic hemispherical contact against a rigid flat. *J Tribol* 2005; 127: 343–354.
9. Jamari J and Schipper DJ. Experimental investigation of fully plastic contact of a sphere against a hard flat. *J Tribol* 2006; 128: 230–235.
10. Chaudhri MM and Yoffe EH. The area of contact between a small sphere and a flat surface. *Philos Mag A* 1981; 44: 667–675.
11. Chaudhri MM, Hutchings IM and Makin PL. Plastic compression of spheres. *Philos Mag A* 1984; 49: 493–503.
12. Zhao Y, Maietta DM and Chang L. An asperity microcontact model incorporating the transition from elastic deformation to fully plastic flow. *J Tribol* 2000; 122: 86–93.
13. Kogut L and Etsion I. Elastic-plastic contact analysis of a sphere and a rigid flat. *J Appl Mech* 2002; 69: 657–662.
14. Quicksall JJ, Jackson RL and Green I. Elasto-plastic hemispherical contact models for various mechanical properties. *Proc IMechE Part J: J Engineering Tribology* 2004; 218: 313–322.
15. Brizmer V, Zait Y, Kligerman Y, et al. The effect of contact conditions and material properties on elastic-plastic spherical contact. *J Mech Mater Struct* 2006; 1: 865–879.
16. Brizmer V, Kligerman Y and Etsion I. The effect of contact conditions and material properties on the elasticity terminus of a spherical contact. *Int J Solids Struct* 2006; 43: 5736–5749.

17. Ovcharenko A, Halperin G, Verberne G, et al. In situ investigation of the contact area in elastic-plastic spherical contact during loading–unloading. *Tribol Lett* 2007; 25: 153–160.
18. Shankar S and Mayuram MM. A finite element based study on the elastic-plastic transition behavior in a hemisphere in contact with a rigid flat. *J Tribol* 2008; 130: 044502–1–044502-6.
19. Wadwalkar SS, Jackson RL and Kogut L. A study of the elastic–plastic deformation of heavily deformed spherical contacts. *Proc IMechE Part J: J Engineering Tribology* 2010; 224: 1091–1102.
20. Cohen D, Kligerman Y and Etsion I. The Effect of surface roughness on static friction and junction growth of an elastic-plastic spherical contact. *J Tribol* 2009; 131: 021404.
21. Li L, Etsion I and Talke FE. Contact area and static friction of rough surfaces with high plasticity index. *J Tribol* 2010; 132: 031401–1–031401-10.
22. Li L, Etsion I and Talke FE. Elastic–plastic spherical contact modeling including roughness effects. *Tribol Lett* 2010; 40: 357–363.
23. Jamari J and Schipper DJ. Deformation due to contact between a rough surface and a smooth ball. *Wear* 2007; 262: 138–145.
24. Shankar S and Mayuram MM. Effect of strain hardening in elastic–plastic transition behavior in a hemisphere in contact with a rigid flat. *Int J Solids Struct* 2008; 45: 3009–3020.
25. Raja KV and Malayalamurthi R. Assessment on assorted hyper-elastic material models applied for large deformation soft finger contact problems. *Int J Mech Mater Des* 2011; 7: 299–305.
26. Long R, Shull KR and Hui C. Large deformation adhesive contact mechanics of circular membranes with a flat rigid substrate. *J Mech Phys Solids* 2010; 58: 1225–1242.
27. Zhao Y and Chang L. A model of asperity interactions in elastic-plastic contact of rough surfaces. *J Tribol* 2001; 123: 857–864.
28. Sahoo P and Banerjee A. Asperity interaction in adhesive contact of metallic rough surfaces. *J Phys D Appl Phys* 2005; 38: 4096.
29. Sahoo P. Adhesive friction for elastic–plastic contacting rough surfaces considering asperity interaction. *J Phys D Appl Phys* 2006; 39: 2809.
30. Ciavarella M, Greenwood JA and Paggi M. Inclusion of "interaction" in the Greenwood and Williamson contact theory. *Wear* 2008; 265: 729–734.
31. Yeo C, Katta R and Polycarpou A. Improved elastic contact model accounting for asperity and bulk substrate deformation. *Tribol Lett* 2009; 35: 191–203.
32. Yeo C, Katta RR, Lee J, et al. Effect of asperity interactions on rough surface elastic contact behavior: hard film on soft substrate. *Tribol Int* 2010; 43: 1438–1448.
33. Mesarovic SD and Fleck NA. Spherical indentation of elastic–plastic solids. *Proc R Soc London Ser A* 1999; 455: 2707–2728.
34. Diegele E, Jansohn W and Tsakmakis C. Finite deformation plasticity and viscoplasticity laws exhibiting nonlinear hardening rules. *Comput Mech* 2000; 25: 1–12.
35. Alcalá J and Esqué-de Los Ojos D. Reassessing spherical indentation: contact regimes and mechanical property extractions. *Int J Solids Struct* 2010; 47: 2714–2732.
36. Jackson RL and Kogut L. A comparison of flattening and indentation approaches for contact mechanics modeling of single asperity contacts. *J Tribol* 2006; 128: 209–212.

Appendix

Notation

A_e	elastic contact area
A_u	the upper limit of contact area
A^*	dimensionless contact area $A/\pi R^2$
A_d^*	dimensionless contact area of deformable base
A_r^*	dimensionless contact area of rigid base
$C_{Ad1} - C_{Ad10}$	coefficients of deformable base area
$C_{Ar1} - C_{Ar8}$	coefficients of rigid base area
Ce_y	factor relates to e_y: $0.14\exp(23e_y)$
$C_{Fd1} - C_{Fd12}$	coefficients of deformable base load
$C_{Fr1} - C_{Fr12}$	coefficients of rigid base load
C_ν	factor relates to ν: $1.295\exp(0.736\nu)$
e_y	yield stress to modulus ratio Y/E'
E	material Young's modulus
E'	equivalent modulus $E/(1-\nu^2)$
F_e	elastic contact load
F^*	dimensionless contact load $F/(\pi Y R^2)$
F_d^*	dimensionless contact load of deformable base
F_r^*	dimensionless contact load of rigid base
H_G	variable hardness of the hemisphere in contact
P	mean contact pressure F/A
R	radius of the hemisphere
V_1	volume of the hemisphere before contact
V_2	volume of the hemisphere after contact
Y	yield stress of material
ν	Poisson's ratio
ω	contact interference
ω_c	critical contact interference
ω^*	dimensionless interference ω/R